



OPEN ACCESS

EDITED BY

Ram Singh,
Instituto Geofísico del Perú, Perú

REVIEWED BY

Subhamoy Chatterjee,
Southwest Research Institute Boulder,
United States
Prithvi Raj Singh,
University of Allahabad, India

*CORRESPONDENCE

R. Selvakumaran,
✉ selva2986@gmail.com
Sneha A. Gokani,
✉ gokanisneha@gmail.com

RECEIVED 30 August 2024

ACCEPTED 21 April 2025

PUBLISHED 09 May 2025

CITATION

Selvakumaran R, Gokani SA and Soni SL
(2025) Detailed understanding of reduced
geoeffectiveness of solar cycle 24 in
association with geomagnetic storms.
Front. Astron. Space Sci. 12:1488696.
doi: 10.3389/fspas.2025.1488696

COPYRIGHT

© 2025 Selvakumaran, Gokani and Soni. This is an open-access article distributed under the terms of the [Creative Commons Attribution License \(CC BY\)](https://creativecommons.org/licenses/by/4.0/). The use, distribution or reproduction in other forums is permitted, provided the original author(s) and the copyright owner(s) are credited and that the original publication in this journal is cited, in accordance with accepted academic practice. No use, distribution or reproduction is permitted which does not comply with these terms.

Detailed understanding of reduced geoeffectiveness of solar cycle 24 in association with geomagnetic storms

R. Selvakumaran^{1*}, Sneha A. Gokani^{1*} and Shirsh Lata Soni²

¹Amity Center of Excellence in Astrobiology, AIB, Amity University Maharashtra, Mumbai, India,

²Department of Climate and Space Science, University of Michigan, Ann Arbor, MI, United States

Solar Cycle 24, the weakest in over a century, exhibited significant deviations from previous cycles, beginning with a prolonged minimum, weak polar fields, and asynchronous polar field reversal, leading to hemispheric asymmetry. Sunspot activity declined by approximately 30% compared to Cycle 23, while the overall occurrence rate of coronal mass ejections (CMEs) decreased, although some studies suggest that the rate of halo CMEs relative to total CMEs may have remained relatively stable. This study investigates the impact of weaker solar activity on geomagnetic storm dynamics by analyzing CME properties, solar wind conditions, and their influence on magnetospheric energy transfer. Key findings indicate that a lower heliospheric pressure in Cycle 24 caused CMEs to expand more than in Cycle 23, altering energy transfer to Earth's magnetosphere. Despite the reduced overall CME rate, the weaker interplanetary magnetic field (IMF) and solar wind pressure led to an 80% reduction in intense geomagnetic storms and a 40% reduction in moderate storms. A detailed epoch analysis revealed a significant delay in the magnetospheric response in Cycle 24 compared to Cycle 23, highlighting the role of weakened solar wind forcing. Furthermore, analysis of the Perrault-Akasofu coupling function (ϵ) showed that the pressure-corrected energy transfer parameter (ϵ^{**}) provides a more accurate estimate of magnetospheric energy input. These findings highlight how reduced heliospheric pressure and weaker solar wind conditions during Solar Cycle 24 significantly influenced geomagnetic storm activity by altering CME expansion and energy transfer to the Earth's magnetosphere, thereby enhancing our understanding of solar-terrestrial coupling processes and improving the predictive capability of space weather models.

KEYWORDS

geomagnetic storms, coronal mass ejection (CME), solar wind magnetosphere coupling, solar cycle, magnetosphere

1 Introduction

Coronal Mass Ejections (CMEs) are large-scale eruptions of plasma and magnetic fields from the Sun's corona that can travel through interplanetary space and interact with planetary magnetospheres, including Earth's. When directed towards Earth, CMEs can cause significant space weather effects, including geomagnetic

storms (Gopalswamy et al., 2000; Webb and Howard, 2012; Chen and Zheng (2013)). The geomagnetic impact of CMEs is largely dependent on their speed, orientation, and the structure of the embedded magnetic fields. CMEs often interact with the solar wind, modifying their propagation characteristics and occasionally producing interplanetary shocks (Gopalswamy et al., 2000; Gonzalez et al., 1994).

The association between CMEs and other solar activities has been extensively studied. While some CMEs are associated with solar flares, not all CMEs originate from flare regions, and the relationship between these two phenomena is complex (Webb and Howard, 2012; Thompson and Myers, 2009). Similarly, filament eruptions often precede CMEs, but their presence is not a strict requirement for CME initiation. Furthermore, while CMEs frequently generate magnetohydrodynamic (MHD) shocks as they propagate through interplanetary space, not all CMEs are associated with MHD shocks (Gopalswamy et al., 2000; Gonzalez et al., 1994). These observations indicate that CMEs are a diverse and dynamic component of solar activity, influenced by multiple factors.

The geoeffectiveness of CMEs is strongly linked to their interaction with Earth's magnetosphere. Historically, CME-driven disturbances have been analyzed through the changes they induce in geomagnetic indices. A critical parameter in this context is the H-component of the geomagnetic field, which reflects the intensity of the horizontal component of Earth's magnetic field and is significantly affected during geomagnetic storms (Kozyra et al., 2003; Daglis et al., 1999; Jordanova et al., 2020). These storms are primarily driven by the interaction between the southward interplanetary magnetic field (IMF) and the Earth's magnetosphere, leading to energy transfer through the process of magnetic reconnection (Dungey, 1961). The primary drivers of geomagnetic storms are the sheaths and magnetic clouds within interplanetary CMEs (ICMEs), with sheath regions often exhibiting higher geoeffectiveness than flux ropes (Huttunen et al., 2002; Huttunen and Koskinen, 2004; Huttunen et al., 2006; Pulkkinen et al., 2005; Tsurutani et al., 2011).

Recent studies comparing Solar Cycles 23 and 24 have shown significant changes in CME properties, highlighting reduced magnetic field strength and heliospheric pressure in Cycle 24 (Manoharan, 2012; Pesnell, 2016; Cliver and von Steiger, 2017). Sunspot activity during Cycle 24 declined by approximately 30% compared to Cycle 23, a reduction linked to the weakened polar magnetic fields during the preceding solar minimum (Schrijver and Liu, 2008; Hathaway and Upton, 2014). Consequently, the heliospheric magnetic pressure and interplanetary magnetic field strength declined significantly during Cycle 24 (McComas et al., 2013; Kakad et al., 2019; Jian et al., 2019). Despite the reduced solar activity, studies have found that the occurrence rate of CMEs remained relatively high during Cycle 24 (Yurchyshyn et al., 2015), with some reports suggesting that CMEs exhibited larger angular widths and anomalous expansion due to weakened heliospheric conditions (Gopalswamy et al., 2014; Gopalswamy et al., 2015a).

The expansion speed of CMEs in Cycle 24 has also been a topic of interest. Dagnew et al. (2020) examined the relationship between radial and expansion speeds of CMEs and found that the slope of this relationship increased by 45% in Cycle 24 compared to Cycle 23, rather than a direct 48% increase in expansion speed. This understanding highlights the importance of considering the

specific velocity ranges when comparing CME properties across solar cycles. Additionally, weaker heliospheric conditions in Cycle 24 contributed to altered CME propagation characteristics, affecting their geoeffectiveness (Gopalswamy et al., 2015a).

Geomagnetic storms caused by CMEs have shown a significant reduction in intensity during Cycle 24. Observations indicate an approximately 80% decrease in intense geomagnetic storms and a 40% decrease in moderate storms compared to Cycle 23 (Selvakumaran et al., 2016). The reduced geoeffectiveness of CMEs in Cycle 24 has been attributed to their anomalous expansion and the lower total plasma and magnetic pressure in the heliosphere (Gopalswamy et al., 2014; 2015a). Furthermore, studies indicate that magnetic cloud structures within CMEs exhibited reduced magnetic content, leading to weaker geomagnetic responses (Gopalswamy et al., 2015a). The weaker solar cycle has also been linked to changes in solar wind structures, including an increase in the magnetopause standoff distance and a decrease in the energy coupling parameter (Kakad et al., 2019). To advance the understanding of CME properties and their space weather effects, it is essential to examine prior research comprehensively. While previous studies have provided valuable insights into CME dynamics and their interaction with Earth's magnetosphere, there is still much to explore regarding their long-term evolution and response to varying heliospheric conditions. This study aims to build upon foundational works (e.g., Huttunen et al., 2002; Pulkkinen et al., 2005; Tsurutani et al., 2011; Gopalswamy et al., 2014; Gopalswamy et al., 2015a; Selvakumaran et al., 2016) and contribute to the broader understanding of how CMEs influence space weather across different solar cycles. By integrating observational data with theoretical models, this research seeks to refine existing frameworks and provide more accurate predictions for future solar cycles.

In this work, we have meticulously identified the solar sources (CMEs) associated with each geomagnetic storm during solar cycles 23 and 24. By comparing these sources, we aimed to uncover the reasons behind the reduced geoeffectiveness observed in cycle 24. Our analysis focuses on the characteristics of the CMEs, such as their speed, magnetic structure, and the resulting energy transfer into the magnetosphere. We also examined how the magnetosphere's response, in terms of energy transfer, differed between the two cycles. This comprehensive approach allows us to establish a clearer connection between the changes in solar eruption propagation through the heliosphere and the subsequent geomagnetic storm activity. By understanding these relationships, we can better predict and mitigate the impacts of space weather events on Earth's technological systems.

2 Data and identification of solar source

The Dst index is used as the primary metric for identifying moderate ($-50 \text{ nT} < \text{Dst} < -100 \text{ nT}$) and intense ($\text{Dst} < -100 \text{ nT}$) geomagnetic storms that occurred during solar cycles 23 and 24 (May 1996 – December 2019). The classification of moderate, intense storms follows the methodology used in González et al. (1994). The Dst index (Disturbance Storm Time Index) is a measure of the intensity of the Earth's ring current, which is influenced by

the interaction between solar wind and the Earth's magnetosphere. It is derived from the horizontal component (H-component) of the geomagnetic field, measured at four low-latitude geomagnetic observatories. A more negative Dst value indicates a stronger geomagnetic storm, as the ring current enhances and depletes the Earth's magnetic field. The Dst index data used in this study is obtained from the World Data Center for Geomagnetism, Kyoto (<http://wdc.kugi.kyoto-u.ac.jp/index.html>). Additionally, storms are considered only if they have recovered to 80% from the prior magnetic field disturbance, ensuring that distinct storm events are analyzed separately.

Geoeffective CMEs are defined as those capable of producing at least a moderate geomagnetic storm. Several methodologies are employed to associate CMEs with specific geomagnetic storms. The solar sources of these CMEs are identified based on flare locations, obtained from the Solar Geophysical Data (SGD) reports (Gopalswamy et al., 2007). The CMEs associated with these flares are identified through running coronagraph image sequences from the Solar and Heliospheric Observatory (SOHO) and the Solar Terrestrial Relations Observatory (STEREO) (http://cdaw.gsfc.nasa.gov/CME_list/index.html). The STEREO mission, which consists of two satellites in Earth's orbit (one leading and one trailing), allows for the continuous tracking of CMEs from the Sun to 1 AU (astronomical unit) during solar cycle 24. The heliospheric imager (HI) onboard STEREO is utilized to correlate the time of density disturbances at 1 AU with CME arrival times, ensuring accurate identification of geoeffective CMEs in solar cycle 24. In some cases where the primary sources did not provide sufficient data, additional source locations were obtained from the Kane and Richardson list (<https://izw1.caltech.edu/ACE/ASC/DATA/level3/icmetable2.html>). The mass and width of geoeffective CMEs were sourced from the CME catalog (http://cdaw.gsfc.nasa.gov/CME_list/index.html), as detailed in Gopalswamy et al. (2009). The solar wind plasma and magnetic parameters, with 1-min resolution, were extracted from CDAWeb (<http://cdaweb.gsfc.nasa.gov/cgi-bin/eval1.cgi>). Due to data gaps in the SOHO mission, the CME association for three moderate and six intense storms could not be determined in solar cycle 23. Similarly, in solar cycle 24, the solar sources for three moderate storms and two intense storms could not be identified. With all the details, the complete catalogue of CME associated geomagnetic storms for solar cycle 23 and 24 is prepared with Dst minimum, source location, CME speed, angular width, ICME type, and magnetospheric input energy. The complete list is given in [Supplementary Table S1](#).

3 Observations and analysis

A total of 257 geomagnetic storms were identified during solar cycle 23 (May 1996 to January 2008) and cycle 24 (April 2008 to December 2019) using the Dst index. Of these, 101 moderate storms and 76 intense storms occurred in cycle 23, while 59 moderate storms and 21 intense storms occurred in cycle 24. The geomagnetic storm catalog ([Supplementary Table S1](#)) for both cycles include details such as the date of occurrence, minimum Dst, solar source location, CME speed, CME angular width, interplanetary magnetic structure, and magnetospheric energy input. The classification of CMEs at 1 AU is based on their magnetic structure, particularly

the presence of a magnetic cloud (MC) or ejecta (EJ) and the associated sheath region. The classification of MC and EJ is based on established *in-situ* criteria such as smooth rotation of the magnetic field, low plasma beta, and enhanced magnetic field strength for MCs, whereas ejecta exhibit irregular magnetic field and plasma signatures. Sheath-only events (S) are characterized by turbulent and compressed solar wind regions without a distinct MC or EJ (e.g., Burlaga et al., 1981; Cane and Richardson, 2003). CMEs with a well-defined MC and sheath are categorized as MC-S, those with an ejecta and sheath as EJ-S, and those consisting primarily of a sheath region without a clear MC or ejecta as S. For cycle 23, we identified 70 MC/MC-S, 82 EJ/EJ-S, and 25S events, while in cycle 24, there were 38 MC/MC-S, 29 EJ/EJ-S, and 13S events. Ejecta-associated structures contributed significantly to geomagnetic storm activity in cycle 23, whereas magnetic clouds were more dominant in cycle 24. [Figure 1](#) illustrates the distribution of geomagnetic storm occurrences in comparison to the Sunspot Number (SSN) for both solar cycles. The storm frequency in cycle 23 follows the SSN trend more closely than in cycle 24, where the peak storm occurrence deviates from the SSN maximum. This discrepancy likely arises from the selective consideration of CME-induced storms and a reduction in the background heliospheric magnetic field, as suggested in previous studies (Gopalswamy et al., 2014; Selvakumaran et al., 2016). These findings indicate variations in the interplanetary conditions influencing geomagnetic storms across the two cycles. Furthermore, the transition from ejecta-driven storms in cycle 23 to magnetic cloud-driven storms in cycle 24 highlights a shift in CMEs and their interactions with Earth's magnetosphere. The reduced heliospheric magnetic field strength in cycle 24 emphasizes the broader solar and heliospheric influences on geomagnetic activity.

3.1 Characteristics changes in solar source properties

[Figure 2](#) illustrates the distribution of CME source locations for Solar Cycles 23 and 24, along with the intensity of the associated geomagnetic storms. Our analysis shows that most intense geomagnetic storms are associated with CMEs originating near the disk center. This is likely because CMEs launched from this region have a higher probability of interacting with Earth's magnetosphere due to their central trajectory. However, CMEs originating from the far disk (closer to the limb) tend to have higher initial speeds on average, which is a crucial factor in generating intense geomagnetic storms. The greater speed of limb-originating CMEs increases their geoeffectiveness by enhancing their ability to compress the magnetosphere upon impact. This distinction emphasizes the dual influence of both the CME's launch position and its initial speed on storm intensity. These observations are consistent with previous studies on moderate geomagnetic storms in the first half of Solar Cycle 24 (Selvakumaran et al., 2016), underscoring the significance of CME source location and speed in determining storm intensity.

[Figure 3](#) presents the distribution of CME speeds associated with moderate and intense geomagnetic storms across both solar cycles, along with the average speeds for each category. Although the number of geoeffective CMEs varies between Solar Cycles 23 and 24, the average CME speeds linked to moderate and intense storms show

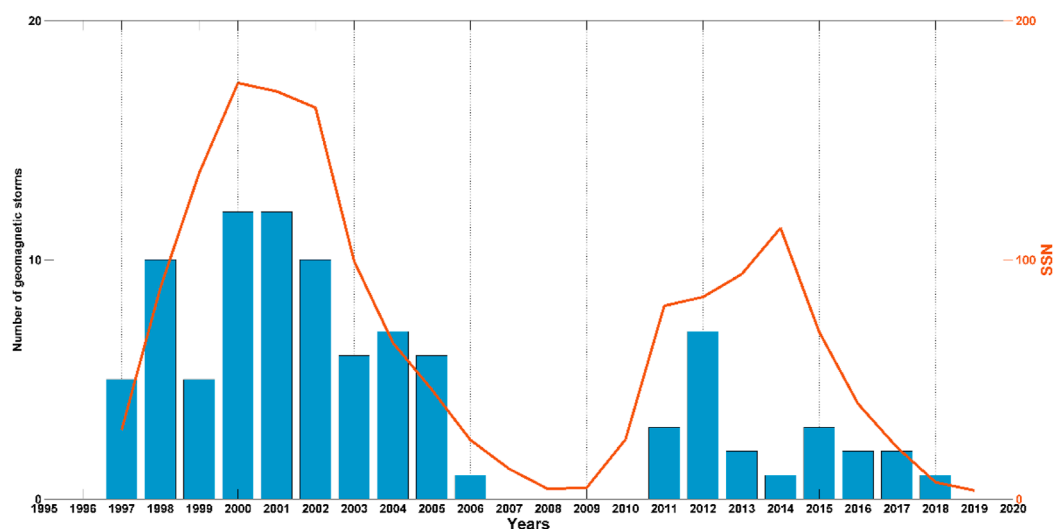


FIGURE 1
Geomagnetic storm occurrences displayed with Sunspot Number (SSN) data for both solar cycles.

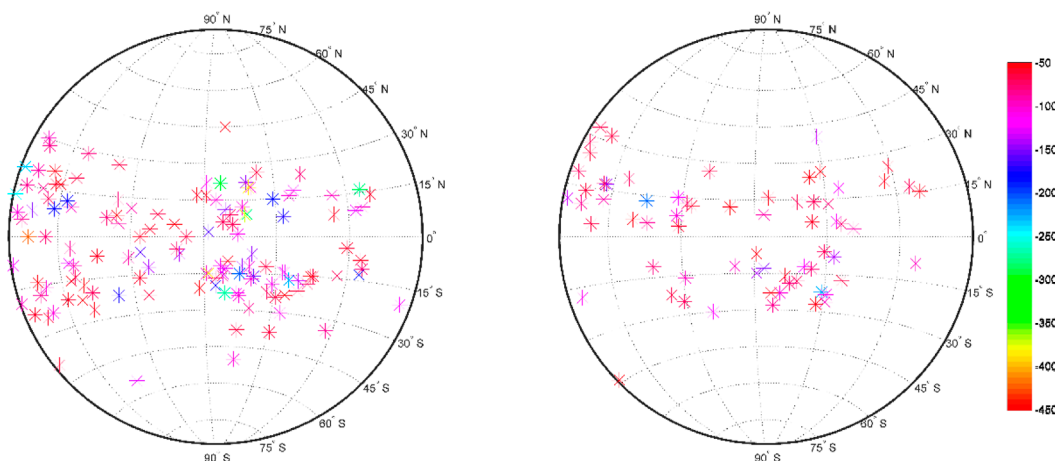


FIGURE 2
CME source locations for Solar Cycles 23 and 24, shown with the intensity of the associated geomagnetic storms. The left panel indicated the source location for solar cycle 23 and right panel for Solar cycle 24.

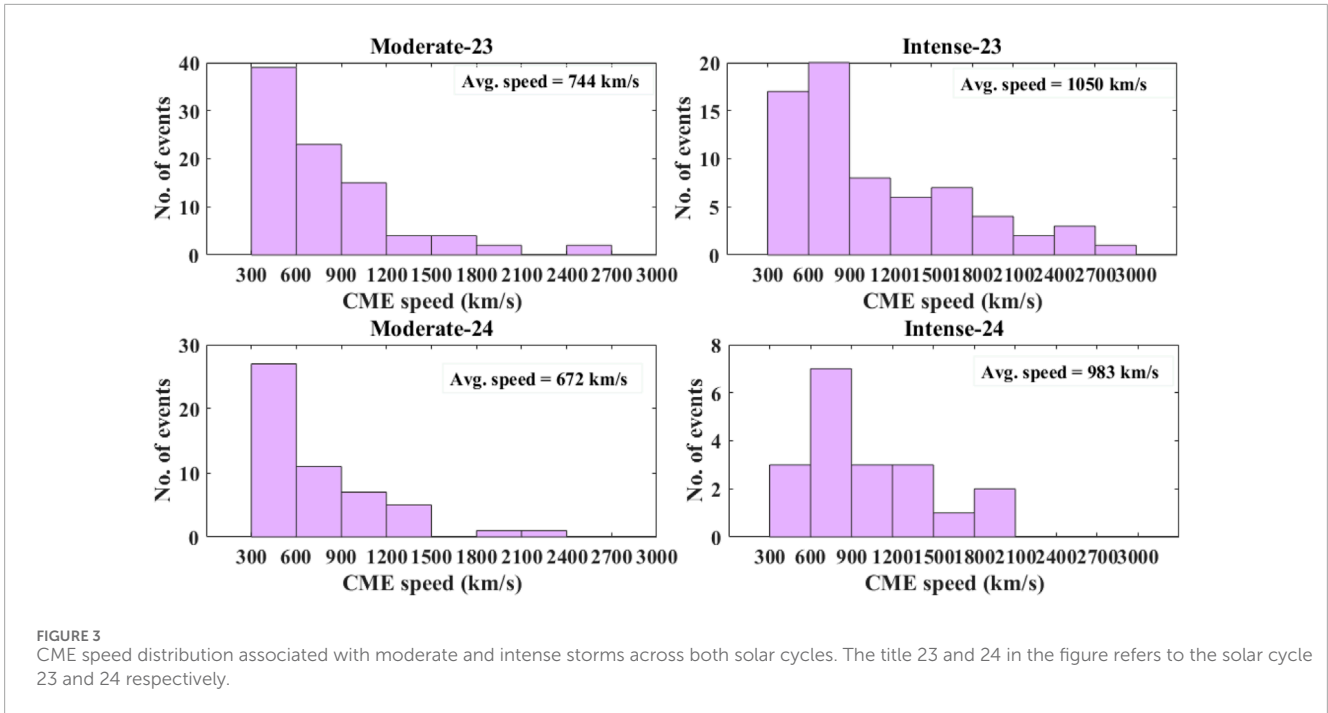
only minor differences, indicating a general consistency between the two cycles. This aligns with earlier reports indicating that the average CME speeds for these storm categories did not significantly change between different phases of the two cycles (Gopalswamy et al., 2014; Gopalswamy et al., 2022; Selvakumaran et al., 2016; Pant et al., 2021). In Solar Cycle 23, 80 geomagnetic storms were associated with halo CMEs, whereas in Cycle 24, 35 such storms were recorded. While some studies suggest anomalous CME expansion during propagation in Cycle 24, the average initial CME width, including halo CMEs, does not differ significantly between the two cycles. The inclusion of halo CMEs in the analysis indicates that the average width of CMEs associated with moderate storms remains largely unchanged between the two cycles (Selvakumaran et al., 2016). This trend holds for all geomagnetic storms, where the average CME width follows a similar pattern to that of moderate

storms (Gopalswamy et al., 2014; Gopalswamy et al., 2015a; Gopalswamy et al., 2015b; Selvakumaran et al., 2016). Thus, despite differences in geomagnetic storm occurrence, the initial physical properties of CMEs, such as their speed and width, remain comparable between the two cycles.

4 Discussion

4.1 Superior magnetosphere energy transfer estimation

The Perrault-Akasofu coupling function (ϵ) is a fundamental parameter used to estimate energy transfer into the magnetosphere during interactions between the solar wind and the Earth's



magnetosphere. This function plays a crucial role in understanding the energy input during extreme space weather events, as it highlights the peak energy transferred into the magnetosphere. However, different versions of ϵ exist, incorporating density and pressure corrections to refine the estimation of magnetospheric energy transfer. To ensure clarity and precision in our analysis, we have introduced the terms ϵ^* for the regular energy estimation and ϵ^{**} for the pressure-corrected estimation. To clarify this distinction, we define ϵ^* and ϵ^{**} using the following equations:

$$\epsilon^* = V B^2 \sin^4(\theta/2) R_{cf}^2$$

$$\epsilon^{**} = V B^2 \sin^4(\theta/2) R_{cf}^2 x f(P)$$

where:

- V is the solar wind speed,
- B is the interplanetary magnetic field (IMF) magnitude,
- R_{cf} is the distance at which the balance between solar wind kinetic plasma pressure and the magnetospheric magnetic pressure
- θ is the IMF clock angle, and
- $f(P)$ is a function that accounts for the solar wind dynamic pressure correction.

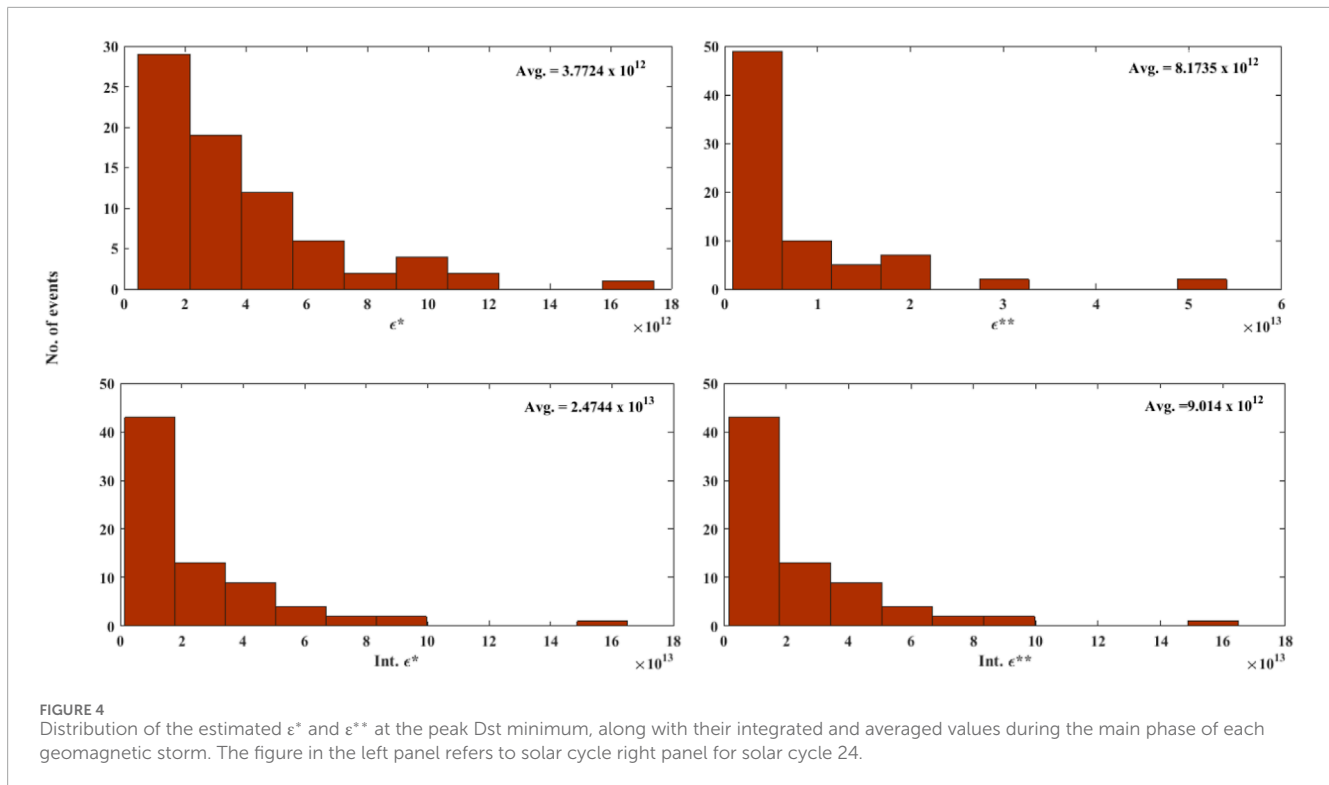
The R_{cf} is given by the equation.

$$R_{cf} = \left(\frac{B_0^2}{4\pi\rho v^2} \right)^{\frac{1}{6}} R_E$$

The pressure correction function $f(P)$ is introduced because previous studies (e.g., Kan et al., 1979; Enford and Østgaard, 2013) have shown that solar wind pressure variations significantly

influence the energy transfer process. The corrected energy transfer function (ϵ^{**}) is expected to provide a more accurate measure of magnetospheric energy input during geomagnetic storms. A detailed examination of energy transfer during the main phase of geomagnetic storms was conducted using these refined coupling functions. Figure 4 illustrates the distribution of estimated ϵ^* and ϵ^{**} values during the peak Dst minimum and their integrated and averaged values throughout each storm's main phase. Notably, the integrated energy transfer values show an order-of-magnitude increase compared to peak estimates, gives the importance of considering both integrated and average energy transfer rather than relying solely on peak values. This observation aligns with the understanding that storm energy is distributed over an extended duration, rather than being concentrated in a single peak event. The total energy transfer is computed by integrating the energy transfer function over the main phase of each storm, from the sudden storm commencement to the minimum Dst index. This calculation helps quantify the overall energy transfer during the storm's progression, with the starting point represented by the sudden storm commencement and the endpoint marked by the time at which the minimum Dst index occurs.

The probability density distributions of ϵ^* and ϵ^{**} for all storms in solar cycles 23 and 24, as shown in Figure 5, highlight the improved confinement of ϵ^{**} . This suggests that the pressure-corrected energy transfer function provides a more consistent and reliable estimation of magnetospheric energy input. The narrower distribution of ϵ^{**} , when compared to ϵ^* , further reinforces its accuracy by demonstrating a reduced standard deviation and an improved correlation with key geomagnetic activity indices. The statistical significance of these findings suggests that ϵ^{**} can serve as a more reliable predictor of energy transfer, especially during major storm events characterized by fluctuating solar wind



conditions. The connection between coronal mass ejections (CMEs) and geomagnetic storms is well-established in space weather studies, with the southward IMF component (B_z) playing a pivotal role in storm intensification. To assess the validity of the refined coupling functions, their correlation with the product of solar wind speed and southward IMF component (V^*B_z) was analyzed. V in different contexts is clarified as follows: when referring to geomagnetic storm drivers, V represents the speed of the solar wind; when considering shock-related influences, V specifically denotes the speed of the shock propagation, which is different from the bulk solar wind speed.

To further ensure the accuracy of the magnetospheric energy input estimation, we examined the relationship between V^*B_z and ϵ^* , ϵ^{**} . The primary relationship between CMEs and geomagnetic storms is driven by the presence of a southward B_z component in the interplanetary magnetic field. This connection has been demonstrated in numerous studies, including those by [Gonzalez et al. \(1994\)](#), [Zhang et al. \(2007\)](#), [Gopalswamy \(2008\)](#), [Echer et al. \(2008a\)](#), [Echer et al. \(2008b\)](#), and [Cid et al. \(2013\)](#). The rate at which the ring current is injected, influencing the storm's overall strength, is determined by V^*B_z , southward B_z duration, and the speed of the shock. The correlation analysis between V^*B_z and the two energy transfer estimates revealed a coefficient of 0.62 for ϵ^* , whereas the correlation with ϵ^{**} improved significantly to 0.75 given in [Figure 6](#). This increase suggests that the pressure-corrected function offers a superior representation of energy input into the magnetosphere, capturing additional variability that is otherwise unaccounted for in traditional estimates. [Figure 7](#) presents ϵ^* , ϵ^{**} , and their ratio, color-coded. V^*B_z and R_{cf} serve as the axes for plotting. The distribution of ϵ^* appears more scattered than that of ϵ^{**} . The ratio highlights the tendency for energy to converge toward

higher values, suggesting that ϵ^{**} provides a better correlation with V^*B_z and R_{cf} .

Coronal Mass Ejections (CMEs) are generally known to follow the solar activity cycle, as indicated by the sunspot number (e.g., [Webb and Howard, 1994](#); [Gopalswamy et al., 2010](#)). However, something peculiar happened during solar cycle 24: space weather became very mild, as evidenced by the paucity of major geomagnetic storms and high-energy Solar Energetic Particle (SEP) events ([Gopalswamy et al., 2014](#); [Gopalswamy et al., 2015a](#)). The number of major geomagnetic storms decreased by a factor of three in cycle 24 compared to the corresponding epoch in cycle 23. Several studies suggest that the diminished solar wind pressure and magnetic pressure were major contributors to the reduced geoeffectiveness observed during solar cycle 24 ([Gopalswamy et al., 2014](#); [Gopalswamy et al., 2015a](#); [Selvakumaran et al., 2016](#); [Kakad et al., 2019](#); [Gopalswamy et al., 2022](#)). Given this reduction in solar activity, accurate energy transfer estimations into the magnetosphere become even more critical. Our findings indicate that the pressure-corrected energy transfer estimation (ϵ^{**}) offers a more precise methodology for assessing magnetospheric energy input. This improved approach provides essential insights into geomagnetic storm dynamics and contributes to the refinement of predictive space weather models, ultimately aiding in the development of strategies to mitigate space weather impacts on technological infrastructure.

4.2 Super epoch analysis

Epoch analysis has become a key tool in the study of geomagnetic storms, providing a means to aggregate and

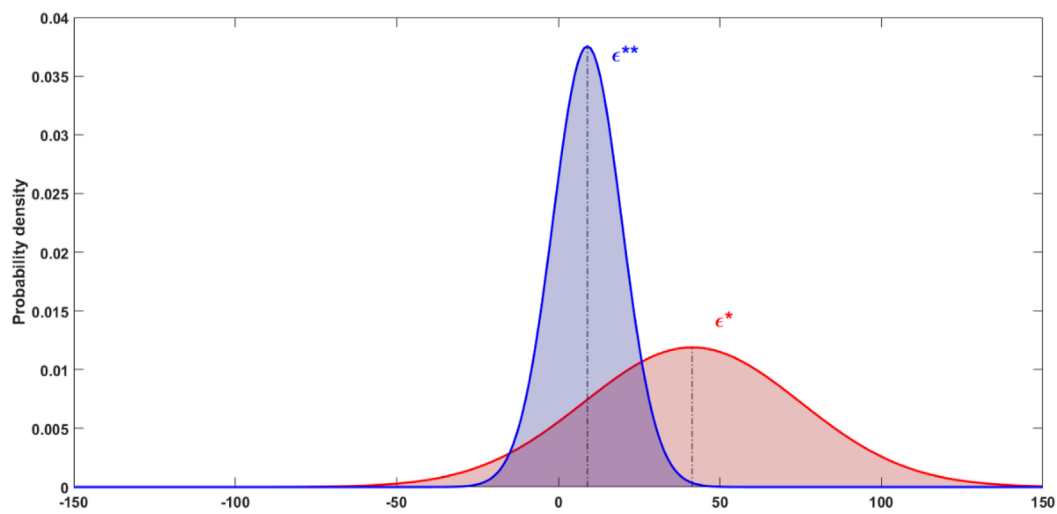


FIGURE 5
Probability density distribution of magnetospheric energy transfer (ϵ^* and ϵ^{**}).

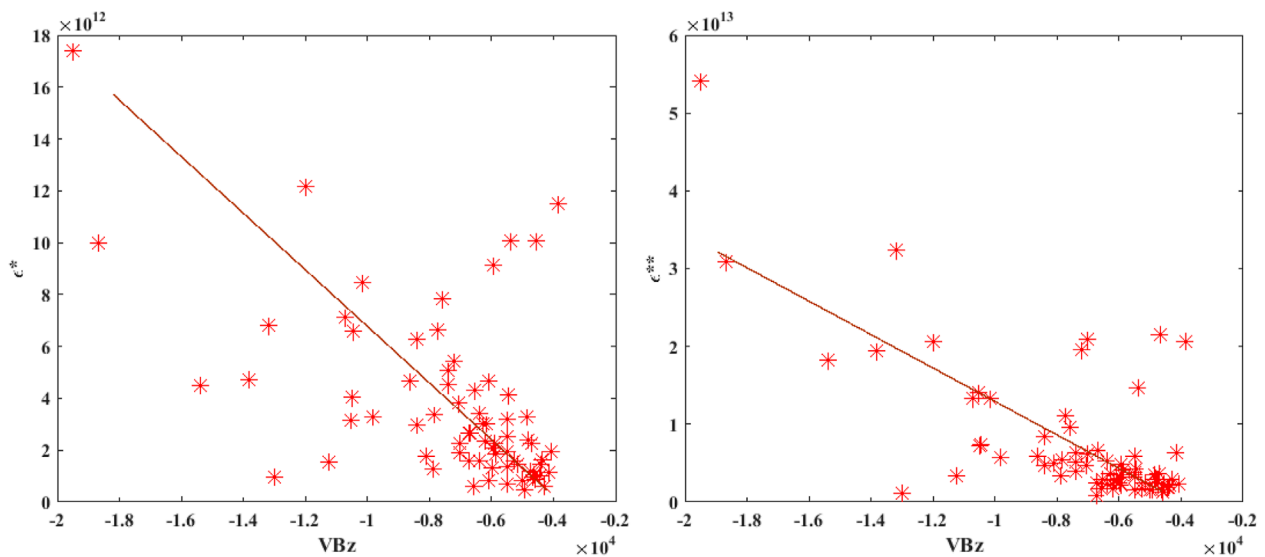
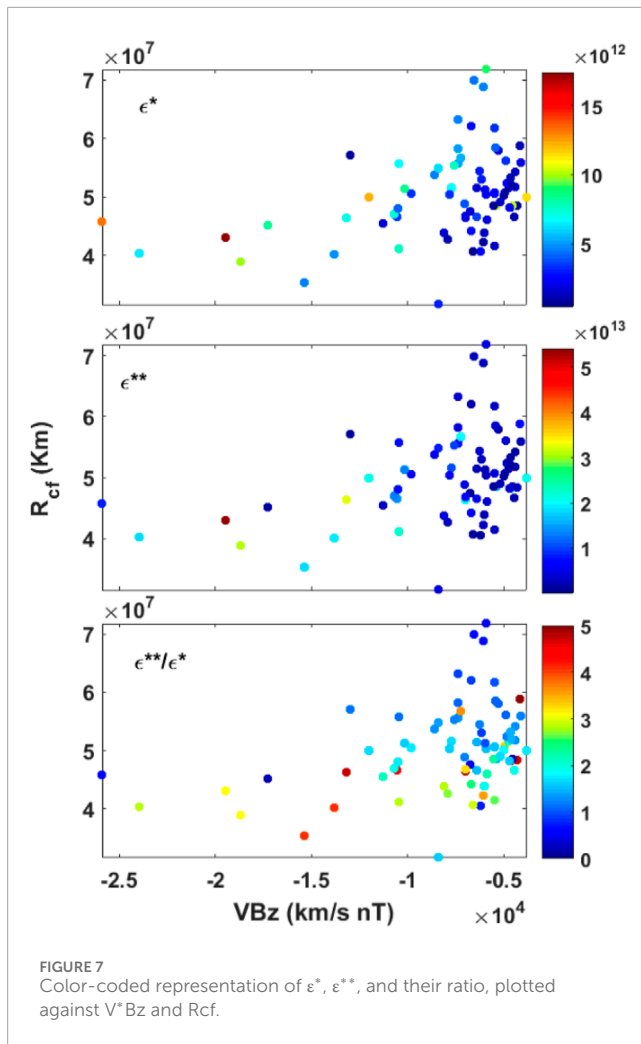


FIGURE 6
Correlation between V^*Bz and ϵ^* and ϵ^{**} for all storms during Solar Cycles 23 and 24. The left panel indicates for solar cycle 23 and right panel for solar cycle 24.

compare multiple storm events to detect common trends and behaviors. This technique involves aligning storm events based on their onset (0 hour), enabling the identification of recurring features and anomalies that might be missed when studying individual storms. Such analysis is crucial for understanding the average behavior of geomagnetic parameters before, during, and after a storm, offering a clearer picture of the overall storm dynamics and their impacts. Furthermore, examining both moderate and intense geomagnetic storms allows for a more comprehensive understanding of how different storm magnitudes influence geomagnetic activity and the Earth's magnetosphere.

Super epoch analysis is carried out for 257 geomagnetic storms that occurred during solar cycles 23 and 24, utilizing both the Dst index and the associated interplanetary electric field (IEFy) to capture the dynamics of geomagnetic disturbances during these periods. This analysis was crucial in offering insights into the behavior of geomagnetic storms across the two solar cycles. As shown in Figure 8, which compares the super epoch analysis for both cycles, the storms from solar cycle 23 are represented on the left, and those from solar cycle 24 are on the right. The black line at 0 hour provides a clear reference point for the onset of the geomagnetic storms, allowing us to track the changes in geomagnetic parameters over time.



The epoch analysis revealed a marked difference in the time taken to reach the average minimum Dst index between the two solar cycles. Specifically, the average minimum Dst for solar cycle 23 was reached within approximately 6 h, while for solar cycle 24, it took almost 15 h to achieve the same minimum. This substantial delay in the magnetospheric response during solar cycle 24 indicates a slower reaction of the Earth's magnetosphere compared to the previous cycle. Such a delay is likely due to several factors, including weakened solar activity and altered heliospheric conditions during solar cycle 24, which have been shown to affect the magnetosphere's response to solar wind pressure (Kalegaev et al., 2014; Kakad et al., 2019; Janardhan et al., 2015). These findings align with the broader understanding that solar cycle 24, which experienced lower solar wind pressure and a reduced background magnetic field in the heliosphere, resulted in a slower magnetospheric response to geomagnetic storms (Liu et al., 2016; Borovsky, 2018). Moreover, studies by Ingale et al., 2019 confirm that solar wind pressure during this period was significantly reduced, which contributed to a slower magnetospheric response compared to earlier cycles.

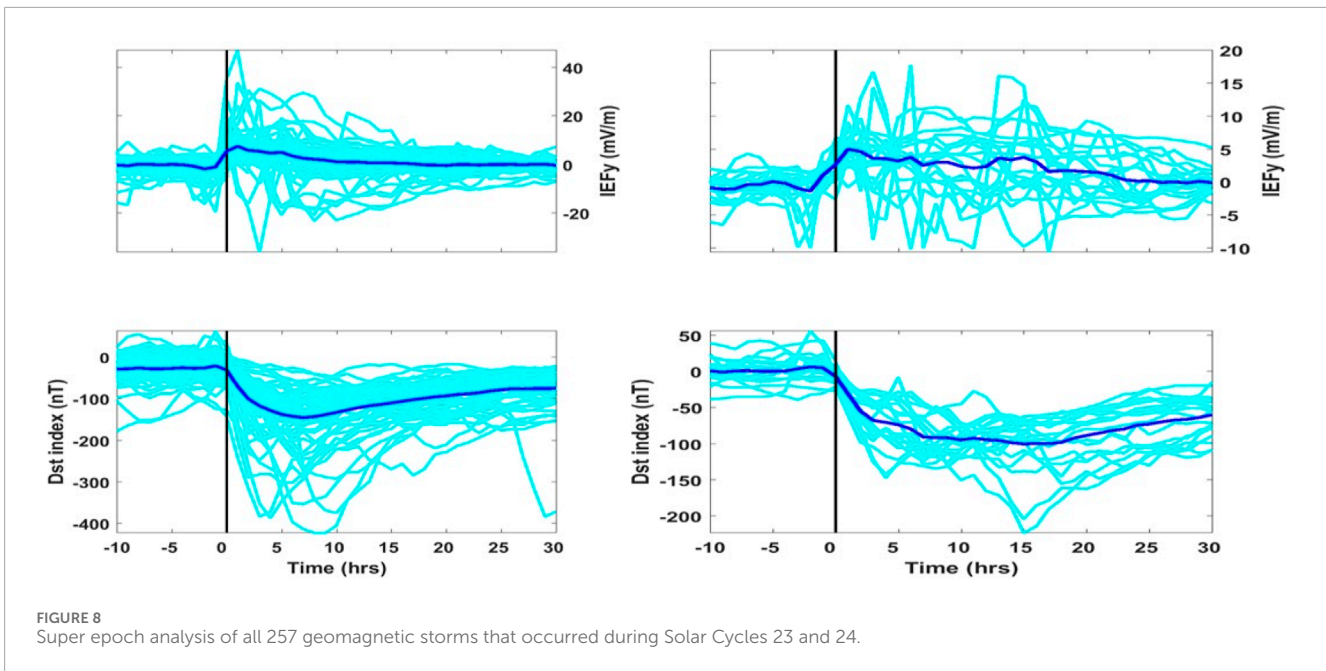
The implications of these delayed responses extend beyond the mere observation of geomagnetic storm timing. The slower reaction of the magnetosphere in solar cycle 24 suggests that the overall stability and intensity of geomagnetic storms may be

influenced by variations in solar and heliospheric conditions. This insight is critical for understanding the long-term behavior of space weather phenomena and their potential impacts on Earth's space environment. Such slower responses could alter the predicted intensity, duration, and impacts of geomagnetic storms, with possible consequences for satellite operations, power grid stability, and other space weather-related technologies. These implications give the importance of further studies and improved forecasting models that can incorporate solar cycle variability when assessing the potential for space weather disturbances (Chen et al., 2015; Kretzschmar et al., 2013; Owens et al., 2021).

In addition to the delay in reaching the minimum Dst index, our analysis also revealed significant changes in the magnetospheric structure during solar cycle 24. The studies by Kakad et al. (2019) and Ingale et al. (2019) suggest that the magnetosphere expanded during solar cycle 24, reaching a local Chapman-Ferraro (LCF) distance of 10.6 Earth radii (RE), compared to 10.2 RE in solar cycle 23 and 9.8 RE in solar cycle 22. This expansion of the magnetosphere is consistent with the observed changes in solar wind pressure and the interplanetary magnetic field (IMF), which directly influence the magnetosphere's response. A deeper understanding of these structural changes is crucial for predicting the impacts of future geomagnetic storms and for designing space weather mitigation strategies (Ferradas et al., 2023). These findings also corroborate with the work of Borovsky, (2018), who demonstrated that variations in solar wind conditions lead to significant structural shifts in the magnetosphere, influencing storm dynamics.

One of the major findings of our study is the estimated 46% reduction in energy transfer to the magnetosphere during solar cycle 24 compared to cycle 23. This reduction was determined by comparing the integrated energy transfer values for both cycles, highlighting a significant decline in magnetospheric energy input. The observed decrease is consistent with previous studies that have reported a weaker heliospheric environment in cycle 24. This reduction in energy transfer has several important implications. Firstly, it has led to a decrease in both the frequency and intensity of major geomagnetic storms, indicating a less active space weather environment. Additionally, the recovery phase for geomagnetic disturbances has become longer, as demonstrated by our super epoch analysis, suggesting that the magnetosphere responds more slowly to perturbations. This reduction in energy transfer has profound implications for the dynamics of geomagnetic storms, affecting their intensity and the extent of the associated disturbances in Earth's magnetosphere. The reduced energy transfer also suggests a less effective coupling between the solar wind and the magnetosphere, a phenomenon that has been studied extensively in other works (Li et al., 2011). The slower buildup of geomagnetic storm intensity during solar cycle 24 further supports these findings, which suggest that weakened solar activity and decreased solar wind pressure can significantly alter space weather dynamics.

Our study builds upon the foundational work of Gopalswamy et al. (2014) and Selvakumaran et al. (2016), while also situating its findings within the broader body of research on geomagnetic storms. Significant contributions from previous studies, including those by Kalegaev et al. (2014), Kakad et al. (2019), and Janardhan et al. (2015), as well as more recent investigations by Kretzschmar et al. (2013), have advanced our



understanding of the magnetospheric response to solar wind variations. Placing our results in this wider scientific context enhances the interpretation of geomagnetic storm dynamics over solar cycles 23 and 24. Furthermore, continuous monitoring and systematic analysis remain essential for refining predictive models of space weather and assessing the impact of solar activity on the Earth's magnetosphere (Kretzschmar et al., 2013; Yermolaev et al., 2021). The findings of Guo et al. (2011) further support this necessity, underscoring the critical role of long-term observations in quantifying the influence of solar activity on geomagnetic storm intensity.

5 Summary and conclusion

This study provides a comprehensive analysis of geomagnetic storm activity during solar cycles 23 and 24, identifying key differences in storm characteristics, energy transfer processes, and the underlying solar drivers. Using the Dst index, a detailed catalog of moderate and intense geomagnetic storms was compiled, documenting critical parameters such as minimum Dst, CME speed, angular width, solar source location, and magnetospheric energy input. A significant shift in the dominant magnetic structure of CMEs at 1 AU was observed, with geomagnetic storms in one cycle primarily driven by ejecta-dominated structures, while magnetic clouds were the predominant drivers in the other. This transition suggests fundamental changes in the nature of solar eruptions and their interaction with Earth's magnetosphere across solar cycles.

A key finding of this study is the variation in the correlation between storm occurrences and Sunspot Number (SSN) across the two cycles. While solar cycle 23 exhibited a strong correlation between SSN and geomagnetic storm frequency, this relationship weakened significantly in cycle 24. This divergence is likely due to the exclusive consideration of CME-associated storms and the overall reduction in the heliospheric magnetic field strength. The observed

shift from ejecta-dominated storms to magnetic cloud-dominated storms, coupled with a decline in background solar wind conditions, underscores the critical role of evolving heliospheric dynamics in modulating geomagnetic activity.

The analysis of CME source locations and kinematic properties provides further insights into storm intensity and geoeffectiveness. It was found that CMEs originating near the solar disk center are more likely to produce intense geomagnetic storms, while those from the far-disk regions tend to have higher initial speeds, influencing their impact on Earth's magnetosphere. Notably, despite significant differences in the frequency and intensity of storms between cycles 23 and 24, the average initial speeds and angular widths of CMEs remained remarkably consistent. This stability suggests that variations in geomagnetic storm intensity and occurrence are not primarily dictated by CME properties alone but are strongly influenced by interplanetary magnetic field variations and solar wind-magnetosphere coupling efficiency.

A crucial contribution of this study is the refined assessment of energy transfer from the solar wind to the magnetosphere using the pressure-corrected Perreault-Akasofu coupling function (ϵ^{**}). This analysis revealed a substantial reduction in magnetospheric energy transfer during cycle 24 compared to cycle 23, primarily due to weakened solar wind pressure and lower interplanetary magnetic field strength. This reduced energy input led to a more expanded magnetosphere and a slower response to geomagnetic disturbances, highlighting the profound impact of heliospheric conditions on storm dynamics.

In conclusion, this study highlights the need for continued research into the varying dynamics of geomagnetic storms across different solar cycles. Understanding the mechanisms behind delayed magnetospheric responses and altered energy transfers is crucial for improving space weather forecasting models and for mitigating the impacts of geomagnetic storms on technological infrastructure. The integration of findings from a diverse range of studies will provide a more comprehensive understanding of how solar and heliospheric

conditions influence geomagnetic activity, ultimately enhancing our ability to predict and respond to space weather phenomena.

6 Summary

Solar Cycle 24 has been observed as the weakest solar cycle in over a century. It commenced with an unusually deep and prolonged minimum following Cycle 23, characterized by a weak polar magnetic field and asynchronous polar field reversal, leading to hemispheric asymmetry (e.g., Manoharan, 2012; Pesnell, 2016; Cliver and von Steiger, 2017). Several observations indicate that the Sun's overall magnetic field was significantly weaker in Cycle 24 compared to previous cycles (e.g., Hathaway, 2015 and references therein). The interplanetary magnetic field also exhibited a substantial decline, leading to the lowest recorded solar wind power. Due to the weak polar magnetic field during the Cycle 23/24 minimum, sunspot activity in Cycle 24 was also diminished, with the sunspot number declining by approximately 30% compared to Cycle 23.

However, the occurrence rate of coronal mass ejections (CMEs) and the number of halo CMEs, which are among the most energetic CMEs, did not show a significant decline in Cycle 24. A notable difference, however, was an 80% reduction in intense geomagnetic storms and a 40% reduction in moderate storms compared to Cycle 23 (Selvakumaran et al., 2016). Gopalswamy et al. (2014) suggested that the reduced geoeffectiveness of CMEs in Cycle 24 was due to lower heliospheric pressure, which caused CMEs to undergo anomalous expansion in the inner heliosphere. This expansion is supported by observations indicating increased CME width beyond a certain distance from the Sun, along with a decrease in total heliospheric pressure (plasma + magnetic). Further, the compression of CMEs closer to the Sun and their subsequent expansion in the inner heliosphere were analyzed to confirm this behavior.

To understand the reduced geoeffectiveness of geomagnetic storms, we analyzed the changes in solar-source flux ropes and their transformation into interplanetary flux ropes, alongside the energy input to the magnetosphere. Utilizing observations from SOHO, STEREO, ACE, and WIND, we identified the solar sources (CMEs) responsible for individual geomagnetic storms in Solar Cycles 23 and 24. This study investigates the characteristics of these sources and their efficiency in transferring energy to the magnetosphere, helping to establish the reasons behind the weaker geomagnetic storm activity in Cycle 24.

Data availability statement

The datasets presented in this study can be found in online repositories. The names of the repository/repositories and accession number(s) can be found in the article/Supplementary Material.

Author contributions

RS Conceptualization, Data curation, Formal Analysis, Investigation, Methodology, Resources, Software, Visualization,

Writing – original draft, Writing – review and editing, Funding acquisition. SG: Conceptualization, Data curation, Formal Analysis, Funding acquisition, Investigation, Software, Validation, Writing – review and editing. SS: Data curation, Formal Analysis, Investigation, Visualization, Writing – review and editing.

Funding

The author(s) declare that financial support was received for the research and/or publication of this article. RS acknowledges the support of the Science and Engineering Research Board, Department of Science and Technology, India, through the research grant PDF/2021/002226. SG carried out this work using the research grant from the Science and Engineering Research Board, Department of Science and Technology, India (2020/RJF/000125).

Acknowledgments

RS extends gratitude to the Space Physics Laboratory (SPL), Vikram Sarabhai Space Centre (VSSC), ISRO, for the assistance provided as part of the NPDF project. RS and SG extend their thanks to Amity University Mumbai for their current employment, which has supported the continuation of this research. The authors would like to express their appreciation to Dr. Gopalswamy and the team at GSFC, NASA, for maintaining the SOHO/LASCO CME catalogue, which was instrumental in this research. We also acknowledge the use of solar imagery provided by the SDO, SOHO, and STEREO missions. Additionally, we thank the NASA OMNI Web team for supplying the IMF and solar wind data at L1.

Conflict of interest

The authors declare that the research was conducted in the absence of any commercial or financial relationships that could be construed as a potential conflict of interest.

Publisher's note

All claims expressed in this article are solely those of the authors and do not necessarily represent those of their affiliated organizations, or those of the publisher, the editors and the reviewers. Any product that may be evaluated in this article, or claim that may be made by its manufacturer, is not guaranteed or endorsed by the publisher.

Supplementary material

The Supplementary Material for this article can be found online at: <https://www.frontiersin.org/articles/10.3389/fspas.2025.1488696/full#supplementary-material>

References

- Borovsky, J. E. (2018). The spatial structure of the oncoming solar wind at Earth and the structure of the magnetosphere. *J. Geophys. Res. Space Phys.* 123 (5), 3837–3870. doi:10.1029/2017JA025102
- Burlaga, L. F., Klein, L., Sheeley, N. R., Michels, D. J., Howard, R. A., Koomen, M. J., et al. (1981). Magnetic cloud at 1 AU. *J. Geophys. Res. Space Phys.* 86 (A8), 6673–6684. doi:10.1029/JA086iA08p06673
- Cane, H. V., and Richardson, I. G. (2003). Interplanetary coronal mass ejections in the near-Earth solar wind during 1996–2002. *J. Geophys. Res. Space Phys.* 108 (A4), 1156. doi:10.1029/2002JA009817
- Chen, J., Kivelson, M. G., and Zong, Q.-G. (2015). The role of solar wind in modulating geomagnetic activity. *J. Geophys. Res. Space Phys.* 120 (8), 6343–6353. doi:10.1002/2015JA021188
- Chen, Y., and Zheng, Y. (2013). On the relation between solar flares and coronal mass ejections: a machine learning approach. *Res. Astronomy Astrophysics* 13 (12), 1509–1518. doi:10.1088/1674-4527/13/12/009
- Cid, C., Palacios, J., Saiz, E., Cerrato, Y., Aguado, J., and Guerrero, A. (2013). Modeling the recovery phase of extreme geomagnetic storms. *J. Geophys. Res. Space Phys.* 118, 4352–4359. doi:10.1002/jgra.50409
- Cliver, E. W., and von Steiger, R. (2017). The extended solar cycle: what have we learned? *Astrophysics Space Sci.* 347 (1), 1–18. doi:10.1007/s10005-017-1088-z
- Daglis, I. A., Thorne, R. M., Baumjohann, W., and Orsini, S. (1999). The terrestrial ring current: Origin, formation, and decay. *Rev. Geophys.* 37 (4), 407–438. doi:10.1029/1999RG900009
- Dagnew, G. K., Gopalswamy, N., and Williams, K. J. H. (2020). Expansion speed of CMEs in solar cycle 24. *Sol. Phys.* 295 (8), 107. doi:10.1007/s11207-009-9464-0
- Dungey, J. W. (1961). Interplanetary magnetic field and the auroral zones. *Phys. Rev. Lett.* 6 (2), 47–48. doi:10.1103/physrevlett.6.47
- Echer, E., Alves, M. V., Batista, I. M. F. S., Alves, J. C. T. M., Queiroz, E. L. G. M., and Silva, V. G. V. (2008a). Geoeffectiveness of interplanetary shocks, magnetic clouds, sector boundary crossings, and their combined occurrence. *J. Geophys. Res. Space Phys.* 113 (A5). doi:10.1029/2008JA013693
- Echer, E., Alves, M. V., Batista, I. M. F. S., Alves, J. C. T. M., Queiroz, E. L. G. M., and Silva, V. G. V. (2008b). Interplanetary conditions causing intense geomagnetic storms ($Dst \leq -100$ nT) during solar cycle 23 (1996–2006). *J. Geophys. Res. Space Phys.* 113. doi:10.1029/2007ja012744
- Enfjord, P., and Østgaard, N. (2013). Energy transfer and flow in the solar wind-magnetosphere-ionosphere system: a new coupling function. *J. Geophys. Res. Space Phys.* 118 (10), 5659–5672. doi:10.1002/jgra.50545
- Ferradas, C. P., Fok, M.-C., Maruyama, N., Henderson, M. G., Califf, S., Thaller, S. A., et al. (2023). The effects of particle injections on the ring current development during the 7–8 September 2017 geomagnetic storm. *Front. Astronomy Space Sci.* 10, 1278820. doi:10.3389/fspas.2023.1278820
- Gonzalez, W. D., Joselyn, J. A., Kamide, Y., Kroehl, H. W., Rostoker, G., Tsurutani, B. T., et al. (1994). What is a geomagnetic storm?. *J. Geophys. Res. Space Phys.* 99 (A4), 5771–5792. doi:10.1029/93JA02867
- Gopalswamy, N. (2008). Solar connections of geoeffective magnetic structures. *J. Atmos. Solar-Terrestrial Phys.* 70 (17), 2078–2100. doi:10.1016/j.jastp.2008.06.010
- Gopalswamy, N., Akiyama, S., Yashiro, S., Xie, H., Mäkelä, P., and Michalek, G. (2014). Anomalous expansion of coronal mass ejections during solar cycle 24 and its space weather implications. *Geophys. Res. Lett.* 41, 2673–2680. doi:10.1002/2014GL059858
- Gopalswamy, N., Alves, M. V., Batista, I. M. F. S., Alves, J. C. T. M., Queiroz, E. L. G. M., and Silva, V. G. V. (2015a). “The solar influence on space weather,” in *Springer handbook of spacetime*. Editors T. B. S., and B. K. (Springer).
- Gopalswamy, N., Alves, M. V., Batista, I. M. F. S., Alves, J. C. T. M., Queiroz, E. L. G. M., and Silva, V. G. V. (2015b). Geoeffectiveness of halo CMEs. *J. Geophys. Res. Space Phys.* 120 (9), 6555–6565. doi:10.1002/2015JA021446
- Gopalswamy, N., Alves, M. V., Batista, I. M. F. S., Alves, J. C. T. M., Queiroz, E. L. G. M., and Silva, V. G. V. (2022). The reduced geoeffectiveness of CMEs in solar cycle 24. *J. Space Weather Space Clim.* 12, A10. doi:10.1002/2014GL059858
- Gopalswamy, N., Lara, A., Lepping, R. P., Kaiser, M. L., Berdichevsky, D., and St. Cyr, O. C. (2000). Interplanetary acceleration of coronal mass ejections. *Geophys. Res. Lett.* 27 (2), 145–148. doi:10.1029/1999GL003639
- Gopalswamy, N., Marubashi, A. R. S. O. K. M., Tsurutani, S. M. M. K., Stenborg, G., Vourlidas, A., Freeland, S., et al. (2009). The SOHO/LASCO CME catalog. *Earth, Moon, Planets* 104, 295–313. doi:10.1007/s11038-008-9282-7
- Gopalswamy, N., Munro, K. T. L., and Howard, J. R. H. N. (2007). Coronal mass ejections, interplanetary magnetic clouds, and geomagnetic storms. *Proc. Int. Astronomical Union* 2 (S235), 399–408. doi:10.1007/s11214-006-9102-1
- Gopalswamy, N., Tsurutani, S. M. M. K., and Cliver, E. W. (2010). CME interactions with coronal holes and their interplanetary consequences. *Adv. Geosciences* 21, 173–184. doi:10.1029/2008JA013686
- Guo, J., Feng, X. S., Emery, B. A., Zhang, J., Xiang, C. Q., Shen, F., et al. (2011). Energy transfer during intense geomagnetic storms driven by interplanetary coronal mass ejections and their sheath regions. *J. Geophys. Res. Space Phys.* 116 (A5). doi:10.1029/2011JA016490
- Hathaway, D. H., and Upton, L. (2014). The solar meridional circulation and sunspot cycle variability. *J. Geophys. Res. Space Phys.* 119, 3316–3324. doi:10.1002/2013JA019432
- Huttunen, K. E. J., and Koskinen, H. E. J. (2004). Importance of post-shock streams and sheath region as drivers of intense magnetospheric storms and high-latitude activity. *Ann. Geophys.* 22, 1729–1738. doi:10.5194/angeo-22-1729-2004
- Huttunen, K. E. J., Koskinen, H. E. J., Karinen, A., and Mursula, K. (2006). Asymmetric development of magnetospheric storms during magnetic clouds and sheath regions. *Geophys. Res. Lett.* 33 (6), L06107. doi:10.1029/2005GL024894
- Huttunen, K. E. J., Koskinen, H. E. J., and Schwenn, R. (2002). Variability of magnetospheric storms driven by different solar wind perturbations. *J. Geophys. Res. Space Phys.* 107 (A7), 1121. doi:10.1029/2001JA900171
- Ingale, M., Janardhan, P., and Bisoi, S. K. (2019). Beyond the minisolar maximum of solar cycle 24: declining solar magnetic fields and the response of the terrestrial magnetosphere. *J. Geophys. Res. Space Phys.* 124, 6363–6383. doi:10.1029/2019JA026616
- Janardhan, P., Bisoi, S. K., Ananthkrishnan, S., Tokumaru, M., Fujiki, K., Jose, L., et al. (2015). A 20 year decline in solar photospheric magnetic fields: inner-heliospheric signatures and possible implications. *J. Geophys. Res. Space Phys.* 120 (8), 5306–5317. doi:10.1002/2015JA021123
- Jian, L. K., Goldstein, M. L., and Phillips, J. L. (2019). Solar cycle dependence of the heliospheric magnetic field strength. *Astrophysical J.* 885 (1), 19. doi:10.3847/1538-4357/ab3e0d
- Jordanova, V. K., Ilie, R., and Chen, M. W. (2020). *Ring Current Investigations: The Quest for Space Weather Prediction*. 1st Edn. Amsterdam: Elsevier. doi:10.1016/B978-0-12-815571-4.00001-9
- Kakad, A., Kakad, B., Ramesh, D. S., and Lakhina, G. S. (2019). Diminishing activity of recent solar cycles (22–24) and their impact on geospace. *J. Geophys. Res. Space Phys.* 127 (5), e2021JA029905. doi:10.1051/swsc/2018048
- Kaleghev, V. V., Zaitsev, M. K., and Khabarova, I. V. (2014). Dynamics of the magnetosphere during magnetic storms. *Geomagnetism Aeronomy* 54 (7), 831–839. doi:10.1002/2015JA021476
- Kan, J. R., and Lee, L. C. (1979). Energy coupling function and solar wind-magnetosphere dynamo. *Geophys. Res. Lett.* 6 (7), 577–580. doi:10.1029/GL006i007p00577
- Kozyra, J. U., Liemohn, M. W., Clauer, C. R., and Ridley, A. J. (2003). Multistep Dst development and ring current composition changes during the 4–6 June 1991 magnetic storm. *J. Geophys. Res. Space Phys.* 108 (A7), 1251. doi:10.1029/2002JA009769
- Kretzschmar, M., Dominique, M., and Dammasch, I. E. (2013). Sun-as-a-Star observation of flares in Lyman α by the PROBA2/LYRA radiometer. *Sol. Phys.* 286, 221–239. doi:10.1007/s11207-012-0175-6
- Li, Y., Luhmann, J. G., Lynch, B. J., and Kilpua, E. K. J. (2011). Cyclic reversal of magnetic cloud poloidal field. *Sol. Phys.* 270, 331–346. doi:10.1007/s11207-011-9722-9
- Liu, Y. D., Hu, H., Wang, C., Luhmann, J. G., Richardson, J. D., Yang, Z., et al. (2016). On sun-to-earth propagation of coronal mass ejections: II. Slow events and comparison with others. *Astrophysical J. Suppl. Ser.* 222, 23. doi:10.3847/0067-0049/222/2/23
- Manoharan, P. K. (2012). Three-dimensional evolution of solar wind during solar cycle 23. *Adv. Space Res.* 49 (4), 522–544. doi:10.1088/0004-637X/751/2/128
- McComas, D. J., Jones, T. H., Williams, N. H., Livadiotis, G., Schwadron, N. A., Skoug, R. M., et al. (2013). Weakest solar wind of the space age and the current “mini” solar maximum. *Astrophysical J.* 779 (1), 2. doi:10.1088/0004-637X/779/1/2
- Owens, M. J., Lockwood, M., Barnard, L. A., Scott, C. J., Haines, C., and Macneil, A. (2021). Extreme space-weather events and the solar cycle. *Sol. Phys.* 296, 82. doi:10.1007/s11207-021-01831-3
- Pant, V., Gupta, A. N., and Sharma, M. K. (2021). Anomalous behavior of solar cycle 24: consequences for solar wind and CME properties. *Mon. Notices R. Astronomical Soc.* 507 (1), 102–112. doi:10.1002/2014GL059858
- Pesnell, W. D. (2016). Predictions of solar cycle 24: how are we doing? *Space weather.* 14 (1), 10–21. doi:10.1002/2015sw001304
- Pulkkinen, A., Lindahl, S., Viljanen, A., and Pirjola, R. (2005). Geomagnetic storm of 29–31 October 2003: geomagnetically induced currents and their relation to problems in the Swedish high-voltage power transmission system. *Space weather.* 3, S08C03. doi:10.1029/2004SW000123
- Schrijver, C. J., and Liu, Y. (2008). The global solar magnetic field through a full sunspot cycle: observations and model results. *Sol. Phys.* 252, 19–31. doi:10.1007/s11207-008-9240-6

- Selvakumaran, R., Veenadhari, B., Ebihara, Y., Hanuise, C., and Singh, R. (2016). Reduced geoeffectiveness of solar cycle 24: comparison with solar cycle 23. *J. Geophys. Res. Space Phys.* 121 (12), 11648–11660. doi:10.1002/2016JA022885
- Thompson, B. J., and Myers, D. C. (2009). A catalog of coronal “EIT wave” transients. *Astrophys. J. Suppl. Ser.* 183, 225–243. doi:10.1088/0067-0049/183/2/225
- Tsurutani, B. T., Lakhina, G. S., Verkhoglyadova, O. P., Gonzalez, W. D., Echer, E., and Guarnieri, F. L. (2011). A review of interplanetary discontinuities and their geomagnetic effects. *J. Atmos. Solar-Terrestrial Phys.* 73, 5–19. doi:10.1016/j.jastp.2010.04.001
- Webb, D. F., and Howard, R. A. (1994). The solar cycle variation of coronal mass ejections and the solar wind mass flux. *J. Geophys. Res. Space Phys.* 99 (A3), 4201–4220. doi:10.1029/93ja02742
- Webb, D. F., and Howard, T. A. (2012). Coronal mass ejections: observations. *Living Rev. Sol. Phys.* 9, 3. doi:10.12942/lrsp-2012-3
- Yermolaev, Y. I., Lodkina, I. G., Dremukhina, L. A., Yermolaev, M. Yu., and Khokhlachev, A. A. (2021). What solar–terrestrial link researchers should know about interplanetary drivers. *Universe* 7 (5), 138. doi:10.3390/universe7050138
- Yurchyshyn, V., Kumar, P., Cho, K.-S., Lim, E.-K., and Abramenko, V. I. (2015). Multiwavelength observations of a slow-rise, multistep X1.6 flare and the associated eruption. *Astrophysical J.* 812 (2), 172. doi:10.1088/0004-637X/812/2/172
- Zhang, J., Zhao, H. L., Wang, Y. G., Li, J. W., Jiang, Y. L., Kasper, J. C., et al. (2007). Solar and interplanetary sources of major geomagnetic storms ($Dst \leq -100$ nT) during 1996–2005. *J. Geophys. Res. Space Phys.* 112. doi:10.1029/2007ja012321